Pergamon

Int. J. Heat Mass Transfer. Vol. 39, No. 7, pp. 1351–1361, 1996

0017-9310/96 $15.00 + 0.00

0017-9310(95)00217-0

Conjugate forced convection in crossflow over a cylinder array with volumetric heating

MINGYU WANG and JOHN G. GEORGIADIS†

Department of Mechanical and Industrial Engineering, University of Illinois at Urbana-Champaign, Urbana, IL 61801, U.S.A.

(*Received* 15 *April* 1994 *and in final form* 21 *June* 1995)

Abstract—Numerical simulation of steady forced convection heat transfer in a laminar flow field over an infinite (periodic) and finite in-line array of cylinders is performed. The cylinders are arranged with a pitch to diameter ratio of two, and are heated internally with a uniform distribution of heat sources. The conjugate heat transfer problem is described by two coupled energy equations (one for the fluid, the other for the solid) and the Navier–Stokes equations. This system is solved on curvilinear coordinates via a finite-difference iterative scheme and a domain decomposition procedure. By varying the ratio of fluid-to-solid thermal conductivity (FS) between 0.01 and 100, a parametric study of heat exchange between the solid and fluid (as expressed by the Nusselt number) is reported for Reynolds numbers between 100 and 400 and Prandtl number equal to 0.71. Our results reveal that the internal heat generation case is profoundly different from that of the isothermal cylindrical array if FS is larger than unity. As FS approaches extreme values, e.g. 0.01 (or 100), the temperature field can be approximated by invoking simpler models, e.g. *local thermal equilibrium* (or *concentric*) model.

1. INTRODUCTION

Lately, conjugate problems have been receiving increasing attention in the heat transfer literature. In this work, we concentrate on the conjugate heat transfer problem involving the coupling of the cool external crossflow with the internal thermal diffusion in volumetrically-heated cylinders in tandem. This problem has important applications in the field of nuclear engineering (reactor safety analysis) and combustion, cf. Golombok *et al.* [1]. Moreover, the study of flows in the interstitial space of a large periodic array of cylinders can provide important clues for the modeling of convective transport in idealized, two-dimensional (2D), fully-saturated packed beds. In the case of a pebble bed reactor, for example, the reactor core consists of a bed of fuel-graphite elements cooled by a downward flow of coolant. During normal operation, the flow is in a forced convection mode, and the core is heated volumetrically by fission.

This model problem is also related to a 2D model for dryout in inductively heated beds of steel spheres fully saturated with a coolant. Another potential application is in the design of the porous flat-plate solar collector. The absorber is a porous plate which heats up as it absorbs incoming radiation and then acts as an internal heat source. Finally, a connection can be established between the model problem and the field of crossflow heat exchangers. This involves the cooling of parallel tubes arranged in periodic patterns, a problem which is reviewed by Zukauskas [2]. The starting point for the study of general problems dealing with crossflow through tube banks has been the consideration of flow over a bank of isothermal cylinders. However, in the majority of cases, the assumption of isothermal boundary conditions is unrealistic. Finite thermal resistance inside the tubes leads to variable temperature profiles in the interior. A complicated conjugate heat transfer problem has to be solved to account for the tube wall and interior–exterior flow. A simpler yet realistic alternative is to solve the conjugate problem involving thermal coupling of heat-generating cylinders with exterior crossflow normal to the cylinders. An internal heat generation term will account for the convective supply of thermal energy due to internal flow.

There is a growing body of literature concerning the hydrothermal field over isothermal, in-line array of spheres and cylinders immersed in crossflow, cf. Dhaubhadel *et al.* [3], Li and Chen [4] and Wung and Chen [5, 6]. In the numerical studies, it is frequently assumed that the flow is steady and symmetric with respect to the centerline of the cylinders in the same row, at least for small to intermediate Reynolds numbers. The same assumption was made in the study of regular arrays of in-line spheres, cf. Tal *et al.* [7–9], Chen and Tong [10]. All the studies consider the forced convection regime in which $(Gr/Re^2) \to 0$. Gr is the Grashof number based on fluid properties and cylinder diameter, cf. Armaly *et al.* [11]. Therefore, the flow is decoupled from the heat transport process and can be studied independently. Baugh and Saniei [12] reported measurements on arrays of cylindrical pin fins with uniform heat flux boundary conditions

†Author to whom correspondence should be addressed.

NOMENCLATURE

a_f, a_s thermal diffusivity of fluid and solid, respectively
C_p heat capacity
D cylinder diameter
FS fluid-to-solid conductivity ratio, FS $= k_f/k_s$
G mean temperature gradient (developed regime), equation (16)
J Jacobian of coordinate transformation
k_f, k_s thermal conductivity of fluid, solid, respectively
L pitch, distance between centers of cylinders in tandem
n unit normal to domain decomposition boundary
Nu average Nusselt number, defined in equation (20)
Nu_l local Nusselt number defined as temperature gradient
Pe Peclet number ($RePr$)
Pr Prandtl number (0.71)
P, Q control function for grid generation
Q_s total heat generation in cylinder
q_s internal heat generation rate per unit volume
Re Reynolds number, UD/ν
t time
T temperature
T_f, T_s temperature in the fluid and in the solid, respectively
$\tilde{T}_{max}-\tilde{T}_{min}$ maximum temperature difference in a block, dimensional
$T_{max}-T_{min}$ maximum temperature difference in a block, scaled with ΔT
u, v velocity component in x, y direction, respectively
U average velocity, $V/(2D)$
V volumetric flow rate per unit depth
x, y streamwise, cross-stream Cartesian coordinates, respectively.

Greek symbols

α $x_\eta^2+y_\eta^2$
β $x_\xi x_\eta+y_\xi y_\eta$
γ $x_\xi^2+y_\xi^2$
ΔT characteristic temperature for scaling, $q_s D^2/k_s$
ρ fluid density
ξ, η coordinates in the computational domain
ν kinematic viscosity
τ unit tangent
ϕ azimuthal position on cylinder perimeter, ($\phi = 0$, upstream stagnation point)
Ψ stream function
ω vorticity.

Subscripts

f fluid
s solid
l local
ξ, η ξ-, η-derivative, respectively.

but these results are beyond the scope of our work since they are exclusively in the turbulent flow regime.

With the exception of the numerical simulation by Kelkar *et al.* [13], there is a lack of studies of forced convection over regular arrays of cylinders with internal heat generation. Wakao *et al.* [14] simply stressed the unreliability of existing experimental data concerning forced convection through packed beds of heat-generating particles. Eichhorn and White [15] employed high-frequency heating to generate heat in spherical particles and reported that the temperature of the particles increases linearly along the flow-direction. In contrast, Balakrishnan and Pei [16] and Bhattacharyya and Pei [17] found that the particle temperature is uniform throughout the bed. Wakao *et al.* [14] reviewed all the available experimental investigations with emphasis on the assessment of validity of various average energy equation models for convection in packed beds. Such models have been built on the equivalence between the real medium and two interspersed fictitious continua which represent the solid and liquid phases. Heat transfer between the phases is explicitly described by an average heat exchange coefficient which is assumed to be only a function of the mean velocity and various geometric parameters of the packed bed. It is our contention that only a direct simulation of the interstitial hydrothermal field can provide a platform for testing such idealizations, cf. Georgiadis [18].

The aforementioned applications and the lack of research in this area provide the main motivation for the fundamental study of convective cooling of heat-generating cylinders in tandem. We consider here an idealized 2D configuration of infinite parallel cylinders subject to crossflow. Owing to the symmetries of the system, we assume that no momentum or energy transfer takes place in the crossflow direction at the streamwise equidistant planes between rows of cylinders. Therefore, it suffices to examine only the flow and temperature fields in a 2D streamwise channel consisting of a single row, as shown in Fig. 1. Two truncated domains are studied: a single-cylinder cell and a five-cylinder channel. The first is relevant in the developed regime; the hydrodynamic field acquires a periodic character in the streamwise direction far from the entrance, cf. Patankar *et al.* [19]. The five-cylinder

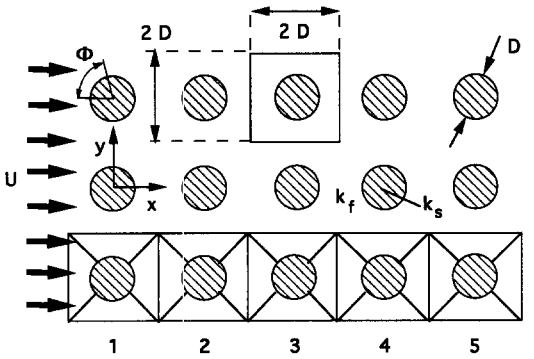

Fig. 1. A periodic bank of heated cylinders in crossflow. Two computational domains are delineated: the upper rectangle marks the periodic regime (1 block). The lower rectangle shows the developing regime at the entrance (5 blocks). The boundaries marking the decomposition of each block into subdomains are also shown.

channel corresponds to the developing regime at the entrance region, and is introduced in order to estimate the effective length of the developing regime.

The present paper is organized as follows. First, the mathematical model is defined in Section 2, and the numerical scheme and method of solution are described in Section 3. Second, results of a simulation of the periodic regime for Reynolds numbers in the range 100–400, and for conductivity ratios from 0.01 to 100, are presented in Section 4.1. Third, the entrance effect is analyzed by simulating forced convection over a five-cylinder array in Section 4.2. Finally, concluding remarks are made in Section 5.

2. MATHEMATICAL FORMULATION

We consider 2D laminar flow around a row of identical cylinders of diameter D and spaced $2D$ apart, as shown in Fig. 1. The governing equations for incompressible flow in streamfunction-vorticity formulation and for forced convective heat transfer are given by:

$$\frac{\partial^2\psi}{\partial x^2}+\frac{\partial^2\psi}{\partial y^2}=-\omega \tag{1}$$

$$\frac{\partial\omega}{\partial t}+\frac{\partial}{\partial x}(u\omega)+\frac{\partial}{\partial y}(v\omega)=\nu\left\{\frac{\partial^2\omega}{\partial x^2}+\frac{\partial^2\omega}{\partial y^2}\right\} \tag{2}$$

$$\frac{\partial T}{\partial t}+\frac{\partial}{\partial x}(uT)+\frac{\partial}{\partial y}(vT)=a_f\left\{\frac{\partial^2 T}{\partial x^2}+\frac{\partial^2 T}{\partial y^2}\right\} \tag{3}$$

$$\frac{\partial T}{\partial t}=a_s\left\{\frac{\partial^2 T}{\partial x^2}+\frac{\partial^2 T}{\partial y^2}\right\}+\frac{q_s}{(\rho C_p)_s}. \tag{4}$$

Equation (4) governs conductive heat transfer within the solid cylinder and equations (1)–(3) describe heat transfer within the fluid-occupied area in the absence of buoyancy forces and radiation effects. Since we consider steady-state fluid flow and heat transfer, the transient terms can be dropped.

The governing equations can be non-dimensionalized by using the diameter D of the cylinder as the characteristic length, the average velocity U in the domain as the characteristic velocity, and $\Delta T = q_s D^2/k_s$ as the characteristic temperature:

$$\frac{\partial^2\psi}{\partial x^2}+\frac{\partial^2\psi}{\partial y^2}=-\omega \tag{5}$$

$$\frac{\partial}{\partial x}(u\omega)+\frac{\partial}{\partial y}(v\omega)=\frac{1}{Re}\left\{\frac{\partial^2\omega}{\partial x^2}+\frac{\partial^2\omega}{\partial y^2}\right\} \tag{6}$$

$$\frac{\partial}{\partial x}(uT)+\frac{\partial}{\partial y}(vT)=\frac{1}{Pe}\left\{\frac{\partial^2 T}{\partial x^2}+\frac{\partial^2 T}{\partial y^2}\right\} \tag{7}$$

$$\frac{\partial^2 T}{\partial x^2}+\frac{\partial^2 T}{\partial y^2}=-1. \tag{8}$$

Any new notation due to non-dimensionalization is suppressed in equations (5)–(8). The streamfunction boundary conditions are given below:

$$\psi = 0.0 \quad \text{on surfaces of cylinders}$$

$$\psi = -0.5 \quad \text{on lower slip wall}$$

$$\psi = 0.5 \quad \text{on upper slip wall}$$

$$\psi(x) = \psi(x+L)$$

for entrance and exit (streamwise periodic condition).

The vorticity boundary conditions are:

$$\omega = 0 \quad \text{on the upper and lower slip wall}$$

$$\omega(x) = \omega(x+L)$$

for entrance and exit (streamwise periodic condition).

The vorticity boundary condition for the cylinder wall is derived by using the Poisson equation for streamfunction and the noslip condition on the wall through the Taylor series expansion technique, see Peyret and Taylor [20]. The temperature boundary conditions are:

$$\frac{\partial T}{\partial n} = 0 \quad \text{on the upper and lower slip wall}$$

where n is normal unit vector to the horizontal upper and lower walls. These are actually symmetry boundary conditions and correspond to an infinite stack of periodic cylinder arrays. The boundary conditions for the temperature field at the entrance and exit need special consideration and will be discussed later.

A composite boundary-fitted grid is used to describe the physical domain, cf. Wang and Georgiadis [21]. The grid is generated numerically based on a coordinate transformation technique developed by Thompson *et al.* [22]. In the curvilinear coordinate system, the governing equations are transformed into the following form:

$$\frac{1}{J^2}\left\{\alpha\frac{\partial^2\psi}{\partial\xi^2}-2\beta\frac{\partial^2\psi}{\partial\xi\,\partial\eta}+\gamma\frac{\partial^2\psi}{\partial\eta^2}+J^2P\frac{\partial\psi}{\partial\xi}+J^2Q\frac{\partial\psi}{\partial\eta}\right\}=-\omega \quad (9)$$

$$\frac{1}{J}\frac{\partial\omega}{\partial\xi}\frac{\partial\psi}{\partial\eta}-\frac{1}{J}\frac{\partial\omega}{\partial\eta}\frac{\partial\psi}{\partial\xi}=\frac{1}{Re\,J^2}\times\left\{\alpha\frac{\partial^2\omega}{\partial\xi^2}-2\beta\frac{\partial^2\omega}{\partial\xi\,\partial\eta}+\gamma\frac{\partial^2\omega}{\partial\eta^2}+J^2P\frac{\partial\omega}{\partial\xi}+J^2Q\frac{\partial\omega}{\partial\eta}\right\} \quad (10)$$

$$\frac{1}{J}\frac{\partial T}{\partial\xi}\frac{\partial\psi}{\partial\eta}-\frac{1}{J}\frac{\partial T}{\partial\eta}\frac{\partial\psi}{\partial\xi}=\frac{1}{Re\,J^2}\times\left\{\alpha\frac{\partial^2T}{\partial\xi^2}-2\beta\frac{\partial^2T}{\partial\xi\,\partial\eta}+\gamma\frac{\partial^2T}{\partial\eta^2}+J^2P\frac{\partial T}{\partial\xi}+J^2Q\frac{\partial T}{\partial\eta}\right\}. \quad (11)$$

Given the geometrical simplicity of the cylinders, we choose the polar coordinate system over the general curvilinear coordinate system for the interior of the cylinder. Two difficulties arise at this point. At the origin of the polar coordinate system ($r = 0$), a mathematical singularity exists which cannot be readily removed when the temperature field lacks centro-symmetry. We have avoided the difficulty by reverting back to the Cartesian coordinate system at the origin.

3. DOMAIN DECOMPOSITION AND NUMERICAL METHOD

In addition to numerical curvilinear coordinate transformation, domain decomposition is used to process the complex geometry introduced in Section 2, following Wang and Georgiadis [21]. The decomposition of the physical domain is carried out on two levels: The domain is first dissected into blocks, as shown in Fig. 1, with each block containing a single cylinder. Second, each of the blocks is further decomposed into four subdomains (of very simple shape) surrounding the cylinder. Owing to the symmetry of the present geometry, the meshing of subdomains is straightforward: only one curvilinear coordinate system is actually generated. For the other three subdomains in the block, a simple rotation of the curvilinear coordinate system by 45° sets up the required coordinate system, as shown in Fig. 2. After a numerical grid is generated for one block, the meshing of the other blocks in the flow field can be completed by horizontal translation.

The method of domain decomposition delineated above suggests a natural way of organizing the data structure for the computation. Our algorithm is constructed around the concept of 'objects'. At the lowest level, the object 'subdomain' is constructed: all the variables describing the curvilinear grid, the flow and the temperature fields in each subdomain are grouped together. At a higher level, the object of 'block' is constructed: each contains one cylinder and is made of five subdomains, four around the cylinder, and the fifth the cylinder itself. At the highest level there is the object of 'field', which is composed of many 'block' objects and constitutes the total computational domain.

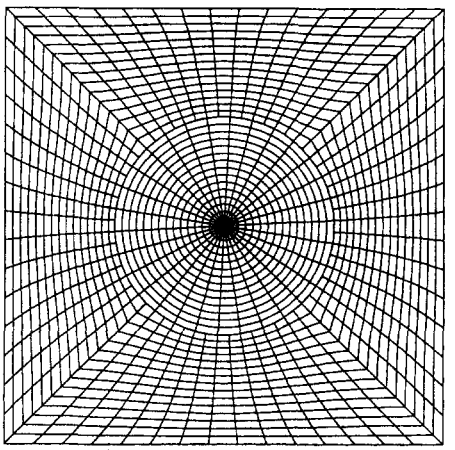

Fig. 2. Numerical grid in a single block. Polar coordinates are used for the cylinder interior.

Since the governing equations in each subdomain are elliptic partial differential equations, conditions need to be imposed on all boundaries to obtain a well-posed problem. In the context of domain decomposition methods, boundary conditions can be classified into two kinds: outer and inner. The outer boundary conditions are those given at the entrance and exit, and on the upper and lower boundaries of the complete computational domain, as discussed in the previous section. The inner boundary conditions are those imposed at the domain decomposition 'cuts'. In the fluid field, the inner boundary conditions for second order partial differential equations, such as equations (5)–(8), are expressed by imposing continuity of each field variable and of the first derivative of each field variable. Mathematically, this expressed as:

$$\frac{\partial f^-}{\partial n}=\frac{\partial f^+}{\partial n} \quad (12)$$

$$\frac{\partial f^-}{\partial\tau}=\frac{\partial f^+}{\partial\tau} \quad (13)$$

where f represents the streamfunction, vorticity or temperature. The $+/-$ signs correspond to the two sides separated by the subdomain boundary, and τ, n are the unit tangent and normal to this boundary, respectively. The inner temperature boundary conditions at the solid–fluid interface are supplied by imposing conservation of heat flux across the interface. This condition, in non-dimensional form, becomes

$$\frac{\partial T_s}{\partial n} = \mathrm{FS}\frac{\partial T_f}{\partial n} \tag{14}$$

where FS is the fluid–solid conductivity ratio, k_f/k_s.

Standard finite-difference approximations are used to discretize the transformed governing equations in each subdomain. The governing equations (9)–(11) are solved iteratively via the Alternating Direction Implicit (ADI) method. With the physical domain properly decomposed and represented, the subdomains serve as the basic units of the simulation. The computation is performed independently in each subdomain and an iterative procedure is set up. This procedure is initiated by assuming a plausible initial guess for the inner boundary data. Equations (9)–(11) are then solved in each subdomain and the inner boundary values are updated by using (12), (13) or (14), depending on whether a fluid–fluid or fluid–solid interface is concerned. This is effectively a fixed-point iteration scheme equivalent to a block Gauss–Seidel method. Although this scheme is amenable to parallelization, cf. Wang and Georgiadis [21], a Cray Y-MP computer in a serial mode is used in this work.

4. RESULTS AND DISCUSSION

Heat transfer is driven by the heat generated inside the solid cylinders. Thermal energy is conducted out of the cylinders and into the fluid, and it is in turn transported out of the domain by conduction and convection through the fluid. The computation is carried out for two regimes: (1) the periodic regime where the field is fully developed and (2) the entrance regime where the flow and temperature fields are spatially developing. Although the study of heat transfer phenomena in the developed regime forms the core of the present work, we also devote some attention to the entrance effect and the associated boundary conditions.

4.1. *Periodic regime*

The streamfunction field for flow at $Re = 100$ is plotted in Fig. 3. The top and bottom boundaries of the domain are subject to the slip condition, which simulates the configuration where identical cylinder arrays are stacked at regular intervals in the y-direction so that periodicity in that direction is established. The entrance and exit of a single cylinder block are subject to the periodicity condition for streamfunction and vorticity. In practice, this periodic flow field can be attained a few cylinder diameters downstream from the entrance region of a cylinder bank.

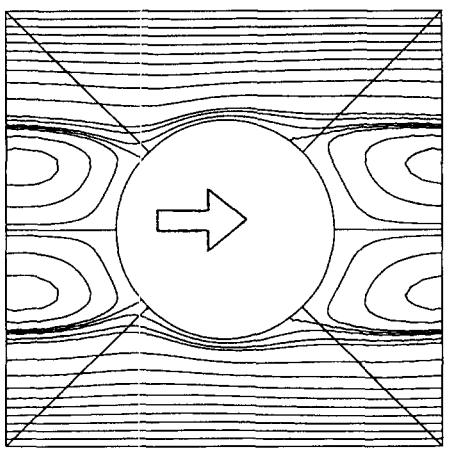

Fig. 3. Periodic flow at $Re = 100$. The streamline contour level is 0.05.

For the temperature field, the infinite extent of the cylinder array in both x- and y-directions implies that the following boundary conditions are pertinent: the top and bottom boundaries are insulated (resulting from symmetry in the y-direction), and the temperature field around the cylinder is fully-developed in the streamwise direction. We have to underline the fact that the characterization 'fully-developed' acquires a special meaning in the case of heat generating cylinders. The temperature profiles at the entrance and exit are not identical: the energy supplied by the cylinder increases the internal energy of the fluid as it flows over the cylinder. Therefore, the temperature at the exit is higher than that at the entrance. The fully-developed condition is implemented with the consideration that, far downstream from the entrance region, the temperature increase in each cylinder block is identical to that of the preceding block. The temperature field can be decomposed into a linear component and a periodic component θ:

$$T(x,y) = Gx + \theta(x,y) \tag{15}$$

where the linear component accounts for the temperature increase due to internal heating, with a gradient G defined as:

$$G = \frac{q_s \pi D^2}{4(\rho C_p)_f LV} \tag{16}$$

and a periodic component:

$$\theta(x,y) = \theta(x+L,y). \tag{17}$$

The decomposition scheme given by (15) was also used by Patankar *et al.* [19].

Figure 4 gives the temperature contour plots for conductivity ratios FS = 0.01, 1, 100, and for Reynolds number $Re = 100$. The isotherms correspond to constant temperature increments. For the lowest conductivity ratio of 0.01, which corresponds to the case of the solid cylinder being much more conductive than the fluid, the temperature in the cylinder is uniform. As will be shown in the following, the temperature differences in the fluid are also small. This complies with the assumption of *local thermal equilibrium* often made in the modeling of heat transfer in fluid-saturated packed beds, cf. Georgiadis [18]. The thermal resistance is exclusively outside the cylinder. When the conductivity ratio is increased to 0.1 and 1.0, the temperature field in the fluid keeps the basic features exhibited by the FS = 0.01 case; there is a well-developed thermal boundary layer near the cylinder

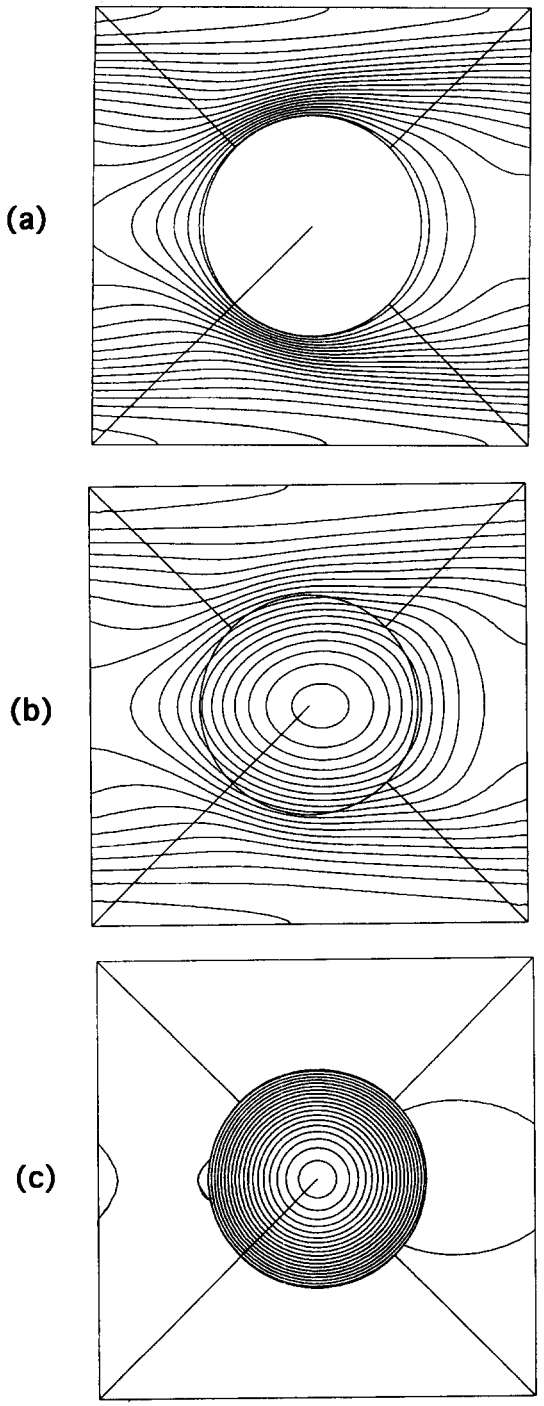

Fig. 4. Effect of conductivity ratio, FS, on the fully-developed temperature field for $Re = 100$. The sum of the periodic and linear temperature components [defined in equation (15)] is plotted. (a) FS = 0.01, (b) FS = 1, (c) FS = 100.

owing to convection. At the same time, important changes are taking place inside the solid cylinder. Owing to the increase in conductivity ratio (resulting from the decrease in the solid conductivity and assuming that the conductivity of the fluid remains constant), the thermal resistance inside the solid cylinder becomes more important, and a temperature gradient in the cylinder becomes gradually established. At FS = 1, the thermal resistance inside and outside the cylinder become balanced; the number of contour lines inside and outside the cylinder are approximately equal to each other.

As the conductivity ratio FS becomes greater than 1 (corresponding to high fluid conductivity or low solid conductivity), the solid cylinder provides most of the thermal resistance. The number of isotherms in the fluid decreases as FS increases, whereas the number of isotherms enclosed by or running through the solid cylinder increases. At FS = 100, the temperature of the fluid is practically uniform. The isotherms in the cylinder take the form of concentric rings. At this limit, the temperature field is consistent with the so-called *concentric model* for packed beds, cf. Wakao *et al.* [14].

The effect of convection is analogous to the effect of conductivity ratio. As the Reynolds number increases, the intensity of the convective heat transfer in the fluid increases. It can be observed that the number of isotherms in the fluid decreases as the Reynolds number is increased from $Re = 100$ in Fig. 4(b), to 200 in Fig. 5(a), and to 400 in Fig. 5(b), all obtained for FS = 1. This trend is true for all conductivity ratios, although it is more obvious for values close to unity. When the conductivity ratio is well above one, the temperature field in the fluid becomes uniform. Thus, convection does not contribute much to the overall heat transfer. When the conductivity ratio is well below one, the cylinder becomes isothermal and major resistance remains in the fluid. Again, the contribution of convection to the overall heat transfer in the fluid (for the range of Reynolds number studied) is not enough to offset the dominance of the high conductivity in the solid cylinder. Only when the conductivity ratio is close to one, convection becomes an effective mechanism for adjusting the distribution of thermal resistance. The proportion of isotherms in the fluid and in the solid becomes sensitive to the intensity of convection.

The effect of convection can be quantified by examining the distribution of local Nusselt number. We define the local Nusselt number as the local temperature gradient normal to the surface of the cylinder:

$$Nu_l = \frac{\partial T}{\partial n}. \tag{18}$$

Figure 6 gives the plots of local Nusselt number vs the azimuthal position ϕ for three conductivity ratios FS = 0.01, 1, 100. The upstream stagnation point on the cylinder corresponds to $\phi = 0$. Owing to the fact that the characteristic temperature used is inversely proportional to the conductivity of the solid, the local Nusselt number defined in (18) is inversely proportional to FS.

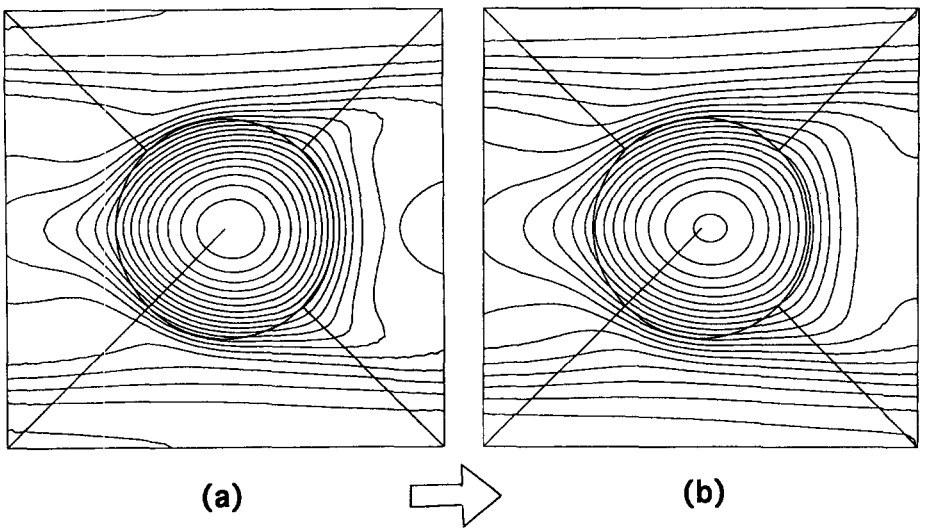

Fig. 5. Effect of Reynolds number on the fully-developed temperature field for FS = 1. The sum of the periodic and linear temperature components [defined in equation (15)] is plotted. (a) $Re = 200$, (b) $Re = 400$.

A common feature in Figs. 6(a)–(c) is that all the curves in each plot have the same mean value. The integral of the local Nusselt number over the wetted cylinder surface gives the total heat generated in the solid cylinder. Any increase in convection can only change the distribution of local heat flux (local Nusselt number). We observe that at the low conductivity ratio FS = 0.01, the local Nusselt number, as defined by equation (18), is a weak function of Reynolds number. In order to explain this, let us note that the temperature of the cylinder is approximately uniform and that the temperature field in the fluid becomes similar to that around an isothermal cylinder array, a problem studied by Tal *et al.* [8], among others. In the case of convective heat transfer around isothermal cylinders, an increase in Reynolds number simply raises the local Nusselt number uniformly, signifying stronger convective heat exchange. In the internal heating case, however, the total heat flux from the cylinder is fixed and convection serves to redistribute weakly the local heat flux. Higher Reynolds numbers produce higher local heat flux intensity near $\phi = 80°$ and 280°, and in the wake region. The local heat flux at the stagnation point of the cylinder is decreased to compensate. For conductivity ratios equal to one and higher, variations in Reynolds number start to affect the distribution of the local Nusselt number. The upstream and downstream stagnation regions have minimum Nusselt values, while maxima occur near $\phi = 90°$ and 270°. As the Reynolds number increases, the azimuthal variation in Nu_l is suppressed.

The definition of local Nusselt numbers given by equation (18) is not practical in the engineering context. The total heat flux from the solid surface is known (since the volumetric heat generation is prescribed). For the temperature field described by (15), a meaningful estimate of the temperature rise within each block can be given by subtracting the lowest temperature (upstream corners of the block boundary) from the maximum temperature (invariably occurring inside the cylinder). This temperature difference obtained from simulation is multiplied by the conductivity ratio, FS, and plotted vs the Reynolds number. The ordinate in Fig. 7 is the nondimensional temperature difference obtained by using the conductivity of the fluid and not that of the solid. This is accomplished by dividing the dimensional temperature difference with $\Delta T_f = q_s D^2/k_f$. With this scaling, we can consider changes in conductivity ratio to occur as a result of increasing or decreasing the solid conductivity, with the fluid conductivity remaining constant. As the conductivity ratio approaches zero (highly conductive solid), the temperature difference of the field is determined only by the thermal resistance of the fluid. This is the lower limit for the temperature difference. When the conductivity ratio is increased above one, the highest temperature gradient shifts to the interior of the solid cylinder (thermal resistance in the solid dominates). The temperature rise in the field increases (without bounds) as the conductivity of the solid decreases. This temperature rise is proportional to FS (or inversely proportional to k_s) and this agrees with the fact that conduction becomes the dominant heat transfer mechanism.

In order to present our results in a more traditional form so as to obtain some comparison with relevant results from the literature, we need to define an average Nusselt number. If we define the heat transfer coefficient, h, by the following relation:

$$Q_s = \frac{\pi D^2}{4} q_s = \pi D h (\tilde{T}_{max} - \tilde{T}_{min}) \qquad (19)$$

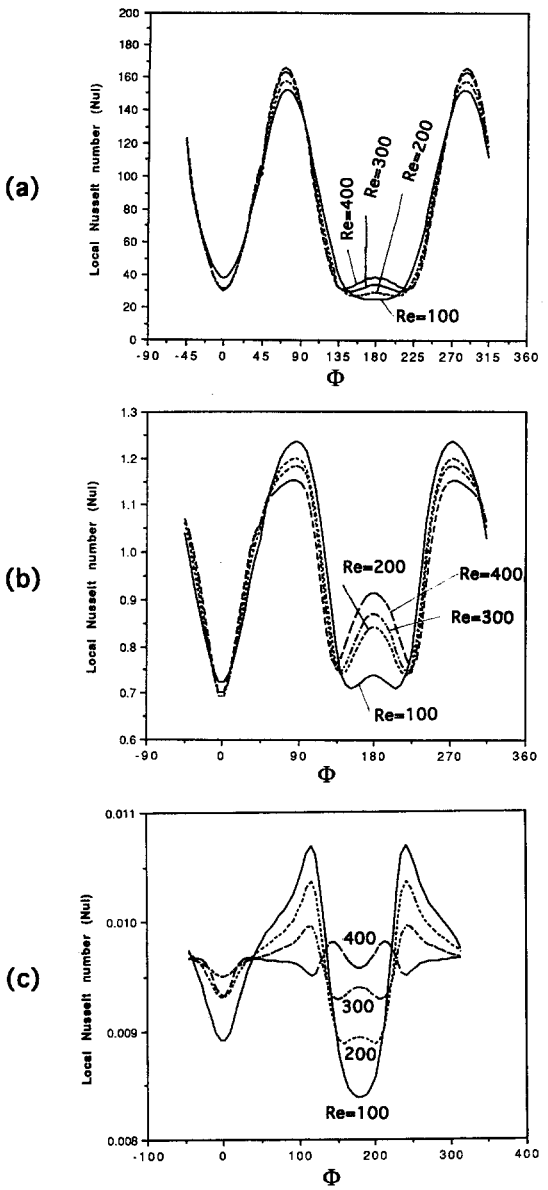

Fig. 6. Distribution of the local Nusselt number on the surface of each cylinder in the developing regime. (a) FS = 0.01, (b) FS = 1, (c) FS = 100.

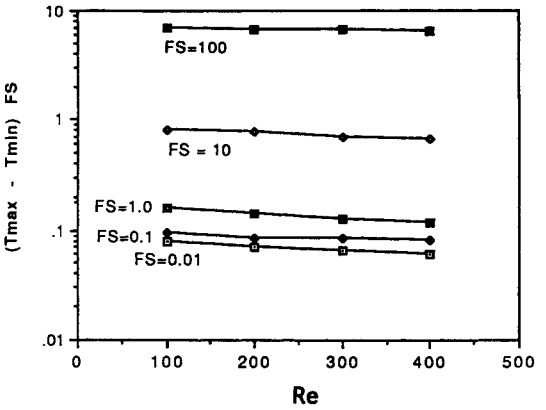

Fig. 7. Plot of temperature rise in a block vs Reynolds number (fully-developed regime) with conductivity ratio, FS, as a parameter.

and the average Nusselt number by:

$$Nu = \frac{hD}{k_f} = \frac{D^2 q_s}{4(\tilde{T}_{max} - \tilde{T}_{min})} \frac{k_s}{k_s k_f} = \frac{1}{4(T_{max} - T_{min})\mathrm{FS}} \tag{20}$$

then the results of Fig. 7 can be modified and tabulated in Table 1 in terms of Nu.

Two trends are apparent by examining Table 1: (1) the Nusselt number increases monotonically with Re at a rate which is a weak function of FS; (2) the Nusselt number decreases strongly as FS increases, especially in the $1 \leqslant \mathrm{FS} \leqslant 100$ range. Only the $0.01 \leqslant \mathrm{FS} \leqslant 1$ regime can be meaningfully related to available results from the literature, since most of available work focuses on flow over isothermal cylinders. There is a similarity between this regime and that for crossflow over isothermal cylinders. Unfortunately, the tube-bank heat exchanger results are not given in a form that is convenient for comparison, cf. Zukauskas [2]. The results of Dhaubhadel *et al.* [3] do not give numerical values for average Nusselt numbers but an estimate can be made from their original figures 6(b) and 6(c): for $Re = 300$, pitch to diameter ratio 1.5, and $Pr = 0.7$, the average Nusselt number for the fifth cylinder is 5.38. When the pitch-to-diameter ratio is changed to 1.8, the average Nusselt number for the same cylinder is 4.4. They postulate that the Nusselt number decreases with the pitch-to-diameter ratio. If the data are extrapolated to pitch-to-diameter ratio of 2.0 (our value), the average Nusselt number is 3.75, which agrees well with our prediction of 3.84 (for FS = 0.01). Other results with local information known to us are for arrays of isothermal spheres. For example, Tal *et al.* [8] predicted $Nu = 5.935$ for periodic flow over an infinite array of isothermal spheres with pitch-to-diameter ratio of 1.5, $Re = 100$, and $Pr = 1$. Tal *et al.* [9] used a two-sphere system with $L/D = 2.5$ and computed $Nu = 3.54$ for the second sphere at $Re = 100$, $Pr = 1$. Our results from Table 1 for FS = 0.01, 0.1 are consistent with the above results, keeping in mind that the latter were obtained for arrays of spheres while our study concerns arrays of cylinders. The wetted area (area exposed to the flow) of a cylinder is 2/3 of that of a sphere with identical volume and diameter. For the same internal heat generation rate, the cylinder develops a larger ΔT, which translates to a lower average Nu than that of a sphere.

A final test of the present results can be obtained by juxtaposing our solution for high FS and Re to the solution of the following simpler problem: a single cylinder (of uniform conductivity and internal heat generation) is exposed to an infinite isothermal fluid, and has a uniform heat transfer coefficient on its surface. To the limit of infinite heat transfer

Table 1. Average Nusselt number as a function of fluid-to-solid ratio (FS) and Reynolds number (Re) for the conjugate heat transfer problem in the developed regime

Re	FS = 0.01	FS = 0.1	FS = 1.0	FS = 10	FS = 100
100	3.171	2.632	1.543	0.309	0.0368
200	3.502	2.887	1.761	0.321	0.0373
300	3.824	2.966	1.984	0.352	0.0375
400	4.152	3.049	2.101	0.368	0.0390

coefficient, the maximum temperature difference (achieved between the center of the cylinder and the surrounding fluid) approaches the value 1/16 (dimensionless). Referring to equation (20) and Table 1, our results for FS = 100 and $Re = 400$ give a value of 1/15.6 for the maximum temperature difference, $T_{max} - T_{min}$. These values are roughly attained at the same points as in the simpler problem, as Fig. 4(c) implies.

4.2. *Developing regime*

In this subsection, we will discuss the developing regime of flow and heat transfer near the entrance of the cylinder array, and for simplicity, we will consider Dirichlet boundary conditions for the entrance, upper and lower boundaries. Several issues need to be addressed, such as the proper outflow boundary conditions, the length needed to reach periodicity (entrance length), and the effect of conductivity ratio.

Traditionally (Tal *et al.* [7], Chen and Tong [10]), the exit boundary conditions for streamfunction, vorticity and temperature field are assumed to be of Neumann type:

$$\frac{\partial f}{\partial n} = 0 \tag{21}$$

where n is the unit normal to the exit, f represents the streamfunction, vorticity or temperature. In our computation, we find that the above condition is acceptable only in terms of the hydrodynamic field (streamfunction and vorticity).

We use equation (21) as the exit boundary condition in the computation of the streamfunction and vorticity field for the five in-line cylinder array. At the entrance to the array, a uniform velocity profile is imposed. On the upper and lower walls, the slip boundary condition is used. We compare this flow field with the periodic flow field discussed in Section 4.1, for $Re = 100$. Periodicity is established starting from the third cylinder. In fact, there are only minor differences between the flow field around the second cylinder and the periodic flow field, which implies that the hydrodynamic entrance length is four cylinder diameters for the above Re. This motivates our assumption that the periodic computation can be used to provide the exit boundary conditions (or to define a 'buffer' domain) for the in-line array. Figure 8 gives the streamfunction distribution with exit boundary conditions obtained from the periodic solution. The streamfunction and vorticity fields resulting from this exit boundary condition agree with the one obtained using (21). According to this criterion, equation (21) is proven to be an adequate exit boundary condition for the flow field.

We have computed the temperature field for conductivity ratios FS = 0.1, 1.0 and 10, and a constant Reynolds number of 100. Figure 9 gives the temperature distribution for crossflow over a five in-line array of cylinders when the conductivity ratio is 1.0. For FS = 0.1, we performed the computation by using both (21) and the periodic field as the exit boundary condition. The local Nusselt numbers from both cases are compared with the periodic regime solution having the same upper and lower wall conditions (Dirichlet). The local Nusselt number profiles on the surface of the last few cylinders converge to the local Nusselt profile for the periodic regime, if the periodic regime solution is used at the exit. In contrast, the profiles obtained using (21) do not converge to the periodic profile. Instead, the local Nusselt number is underpredicted. We conclude that for exit condition for the temperature field, the periodic boundary condition is preferable.

Figure 10(a) depicts the local Nusselt number profiles on the surfaces of the five in-line cylinders for

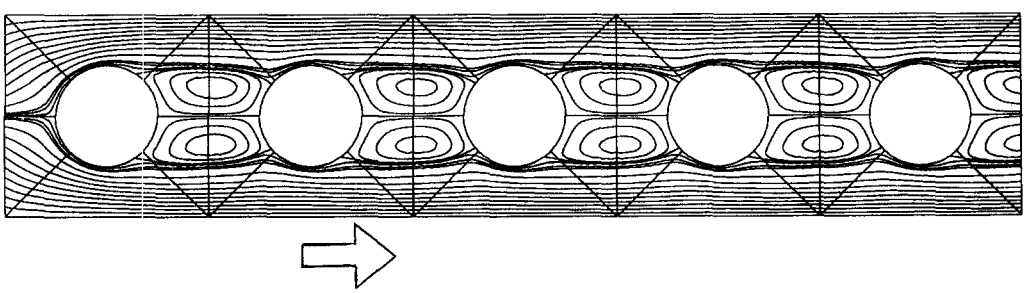

Fig. 8. Flow field in the entrance region with periodic exit boundary condition for $Re = 100$ and FS = 1.

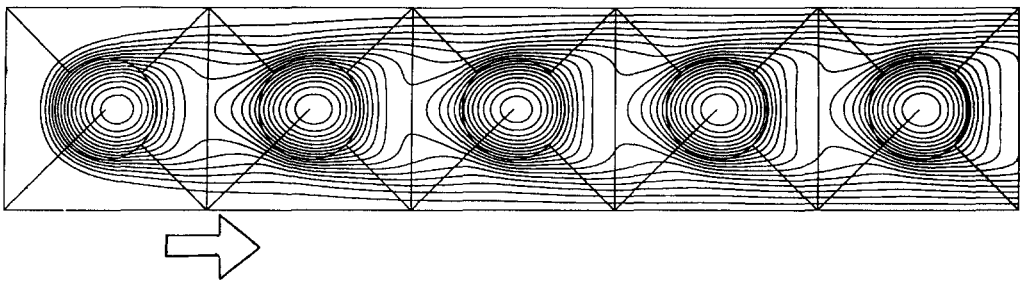

Fig. 9. Temperature field in the developing regime with periodic exit boundary condition for $Re = 100$ and FS = 1.

FS = 0.1. We can see that the first cylinder has a Nu_1 profile which differs significantly from that for the other cylinders. The front of the first cylinder, which faces the incoming cold fluid, exhibits a uniform Nusselt number distribution typical of stagnation flow. Starting from the wake of the first cylinder, the local Nusselt number acquires a typical oscillatory shape. The profiles of the last four cylinders converge into a limit profile, indicating developed periodic regime. This lends support to the conjecture made by Cheng and Tong [10] (who studied the analogous flow around arrays of in-line spheres) that periodicity can be expected after the first sphere. Figure 10(b) is the local Nusselt number distribution when the conductivity ratio is 1. At this conductivity ratio, the temperature field becomes periodic at larger distances. Both the first and the second cylinders have profiles tangibly different from those succeeding them. When FS is greater than one, the temperature field does not seem to develop into the periodic regime within five cylinders, as shown in Fig. 10(c). The last result should be considered with caution, since periodic exit conditions are used while streamwise periodicity does not develop.

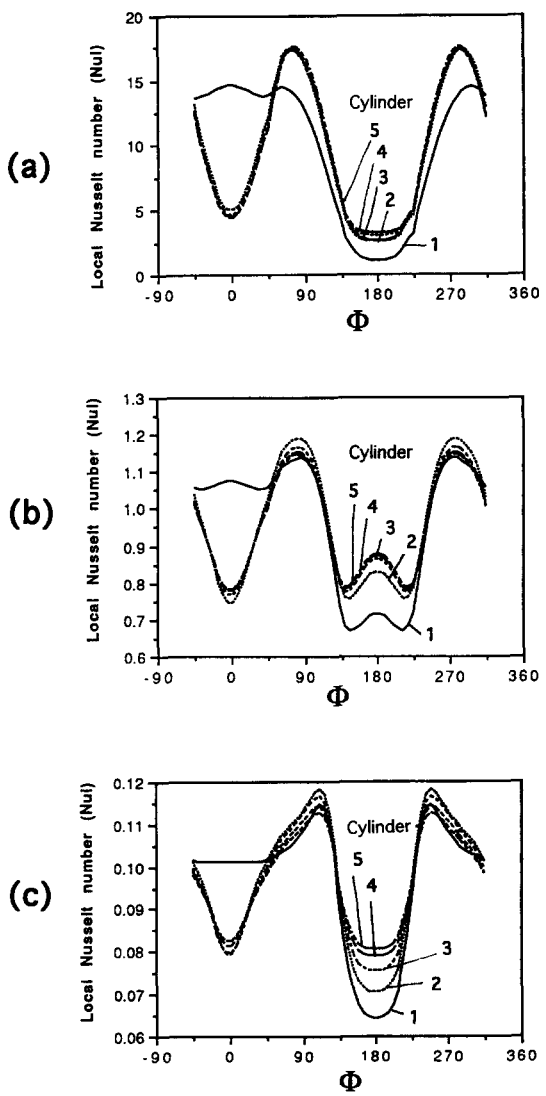

Fig. 10. Local Nusselt number distribution in the developing regime. (a) FS = 0.1, (b) FS = 1, (c) FS = 10.

5. CONCLUSIONS

The phenomena of heat transfer and fluid flow around arrays of cylinders in crossflow are important in regard to many engineering applications. The present work extends earlier research on convective heat transfer of isothermal cylinders by studying a conjugate problem involving a heat generating cylinder array located in crossflow. Both the developed and entrance regimes have been investigated using the method of domain decomposition based on numerical grid generation and finite difference discretization. The investigation demonstrates that the numerical scheme used here is flexible in handling the complex geometry as well as different material properties in the field.

We can briefly summarize our heat transfer results as follows:

(1) Developed (periodic) regime: the temperature rise for fixed internal heating rate decreases monotonically with Reynolds number but increases with the fluid-to-solid conductivity ratio, FS.

(2) Developing regime: the hydrodynamic entrance length is about two-cylinders long. The thermal entrance length depends on the conductivity ratio. The entrance regime is only two cylinders deep when FS = 0.1, but becomes deeper as FS increases.

(3) Exit boundary conditions: the Neumann-type boundary condition is satisfactory as far as the hydrodynamic field is concerned, while a temperature exit boundary condition based on the periodic regime (buffer domain) solution is generally preferable.

(4) Comments regarding packed bed models: the concentric model of Wakao *et al.* [14] seems to be a good approximation for FS values larger than 10. On the other hand, the temperature differences between solid and fluid are small for FS < 0.1, which is in compliance with the local thermal equilibrium assumption.

Acknowledgements—Mingyu Wang would like to thank the NIH/NSF Engineering Research Center for Emerging Cardiovascular Technologies at Duke University for financial support. The work of John Georgiadis was partially supported by the National Science Foundation (grants CTS-8909119 and CTS-9006189). Both authors are also indebted to the North Carolina Supercomputing Center for a generous allocation of computing resources.

REFERENCES

1. M. Golombok, J. Jariwala and L. C. Shirvill, Gas–solid heat exchange in a fibrous metallic material measured by a heat regenerator technique, *Int. J. Heat Mass Transfer* **33**(2), 243–252 (1990).
2. A. Zukauskas, Heat transfer from tubes in crossflow, *Adv. Heat Transfer* **18,** 87–159 (1987).
3. M. N. Dhaubhadel, J. N. Reddy and D. P. Telionis, Penalty finite-element analysis of coupled fluid flow and heat transfer for in-line bundle of cylinders in cross flow, *Int. J. Nonlinear Mech.* **21,** 361–373 (1986).
4. J. W. Li and M. M. Chen, Computations of 2-D and 3-D regular arrays of cylinders and spheres in a flow field. In *Convective Heat Transfer in the Presence of an Obstructing Medium*, HTD-Vol. 144 (1990).
5. T.-S. Wung and C. J. Chen, Finite analytic solution of convective heat transfer for tube arrays in crossflow—I. Flow field analysis, *J. Heat Transfer* **111,** 633–649 (1989).
6. T.-S. Wung and C. J. Chen, Finite analytic solution of convective heat transfer for tube arrays in crossflow—II. Heat transfer analysis, *J. Heat Transfer* **111,** 641–648 (1989).
7. R. Tal, D. N. Lee and W. A. Sirignano, Hydrodynamics and heat transfer in sphere assemblages—cylindrical cell models, *Int. J. Heat Mass Transfer* **26,** 1265–1273 (1983).
8. R. Tal, D. N. Lee and W. A. Sirignano, Periodic solution of heat transfer for flow through a periodic assemblage of spheres, *Int. J. Heat Mass Transfer* **27,** 1414–1417 (1984).
9. R. Tal, D. N. Lee and W. A. Sirignano, Heat and momentum transfer around a pair of spheres in viscous flow, *Int. J. Heat Mass Transfer* **27,** 1953–1962 (1984).
10. S. Chen and A. Y. Tong, Application of elliptic grid generation technique to the solution of hydrodynamics and heat transfer of droplet arrays at intermediate Reynolds numbers, *Int. J. Heat Mass Transfer* **31,** 1065–1072 (1988).
11. B. F. Armaly, T. S. Chen and N. Ramachandran, Correlations for mixed convection flows across horizontal cylinders and spheres, *J. Heat Transfer* **110,** 511–514 (1988).
12. J. W. Baughn and N. Saniei, Local heat transfer measurements on arrays of pin fins in a rectangular duct, *Proceedings of the 9th International Heat Transfer Conference* (Edited by G. Hetsroni), Vol. 5, pp. 39–44 (1990).
13. K. M. Kelkar, D. Choudhury and M. Ambrosi, Numerical method for the computation of conjugate heat transfer in nonorthogonal boundary-fitted coordinates, *Numer. Heat Transfer B* **20**(1), 25–40 (1991).
14. N. Wakao, S. Kaguei and T. Funazkri, Effect of fluid dispersion on particle-to-fluid heat transfer coefficients in packed beds, *Chem. Engng Sci.* **34,** 325–336 (1979).
15. J. Eichhorn and R. R. White, *Chem. Engng Prog. Symp. Ser.* **48** (4), 11 (1952).
16. A. R. Balakrishnan and D. C. T. Pei, *Ind. Engng Chem. Proc. Des. Dev.* **13,** 441 (1974).
17. D. Bhattacharyya and D. C. T. Pei, *Chem. Engng Sci.* **30,** 293 (1975).
18. J. G. Georgiadis, Future research needs in heat and mass transport in porous media. In *Convective Heat and Mass Transfer in Porous Media* (Edited by S. Kakaç, B. Kilkis, F. A. Kulacki and F. Arinç), NATO Advanced Study Institute Series, Vol. E 196, pp. 1073–1088. Kluwer Academic, The Netherlands (1991).
19. S. V. Patankar, C. H. Liu and E. M. Sparrow, Fully developed flow and heat transfer in ducts having streamwise-periodic variations of cross-sectional area, *J. Heat Transfer* **99,** 180–186 (1977).
20. R. Peyret and T. D. Taylor, *Computational Methods for Fluid Flow*. Springer, New York (1983).
21. M. Wang and J. G. Georgiadis, Parallel computation of forced convection using domain decomposition, *Numer. Heat Transfer B,* **20**(1), 41–60 (1991).
22. J. F. Thompson, Z. U. A. Warsi and C. W. Mastin, Boundary-fitted coordinate systems for numerical solutions of partial differential equations—a review, *J. Comput. Phys.* **47,** 1–108 (1982).